九州大学学術情報リポジトリ
Kyushu University Institutional Repository

Effect of Size-Controlled Graphene Quantum Dots Combined with Ni(OH)_2 for Supercapacitor Application

Tibodee, Ananya
Department of Chemistry and Centre of Excellence for Innovation in Chemistry, Faculty of Science, Kasetsart University

Thaweechai, Thammanoon
Department of Chemistry, Faculty of Science, Kasetsart University

Sirisaksoontorn, Weekit
Department of Chemistry and Centre of Excellence for Innovation in Chemistry, Faculty of Science, Kasetsart University

https://doi.org/10.15017/1961304

出版情報：Proceedings of International Exchange and Innovation Conference on Engineering & Sciences (IEICES). 4, pp.127-129, 2018-10-18. 九州大学大学院総合理工学府
バージョン：
権利関係：

Effect of Size-Controlled Graphene Quantum Dots Combined with Ni)OH(2 for Supercapacitor Application

Ananya Tibodee[1], Thammanoon Thaweechai[2], Weekit Sirisaksoontorn[1,*]
[1]Department of Chemistry and Centre of Excellence for Innovation in Chemistry, Faculty of Science, Kasetsart University, Chatuchak, Bangkok 10900 Thailand
[2]Department of Chemistry, Faculty of Science, Kasetsart University, Chatuchak, Bangkok 10900 Thailand
*Corresponding author: fsciwks@ku.ac.th

Abstract: The composites of $Ni(OH)_2$/GQDs were prepared via a hydrothermal method and tested as electrode materials for electrochemical capacitors. The as-prepared products were characterized by X-ray diffraction (XRD) and scanning electron microscopy (SEM). The electrostatic forces between GQDs and $Ni(OH)_2$ facilitate the self-assembly of the $Ni(OH)_2$/GQD composites. Furthermore, the composites were electrochemically tested by cyclic voltammetry, galvanostatic charge/discharge and electrochemical impedance spectroscopy. The $Ni(OH)_2$/GQD composite with a smaller size of GQD provides the better electrochemical performance compared to $Ni(OH)_2$ and $Ni(OH)_2$/GQD with a larger size of GQD. The $Ni(OH)_2$/GQD composite exhibits the high specific supercapacitance of 1487 F g^{-1} at a current density of 2 A g^{-1} in 2 M KOH electrolyte.

Keywords: Graphene quantum dots, Ni**(**OH**)**$_2$ nanoflower, Supercapacitor

1. INTRODUCTION

Supercapacitors (SCs), also known as ultracapacitors or electrochemical capacitors, have many advantages for energy storage due to their high power density, long cycle life, low maintenance cost and environmentally eco-friendly nature. In general, SCs can be classified into two categories based on their energy storage mechanisms. First, the electrical double-layer capacitors (EDLCs) store charge via fast reversible charge adsorption/desorption of the electrolyte ions onto the surface of active materials. The carbonaceous materials such as activated carbon, graphene and carbon nanotube have been widely used as electrodes in EDLCs. Second, pseudocapacitors are capable of storing charge via the faradaic reactions which are related to the electron transfer process on the electrode materials. Transition metal oxide/hydroxide and conductive polymers are considered to be a major component for the electrode fabrication [1].

Graphene quantum dots (GQDs), as a zero-dimensional (0D) carbon nanomaterial, consist of nanometer-scaled graphene particles. GQDs with a nanoscale size can be well-dispersed in various organic solvents. GQDs have tremendous interest owing to its electronic properties, quantum confinement and edge effects. Because of those exciting properties, GQDs have emerged as promising materials for supercapacitors, batteries, optoelectronics and biomedical field [2].

$Ni(OH)_2$ mainly consists of the stacking sequence of octahedral layers. There are two known polymorphs such as α-$Ni(OH)_2$ and β-$Ni(OH)_2$. α-$Ni(OH)_2$ or $Ni(OH)_2 \cdot xH_2O$ ($0.41 \leq x \leq 0.70$) contains β-$Ni(OH)_2$ layers which are randomly stacked along the c-axis with the insertion of anion and water molecules in the interlayer space. This structure is also known as a hydrotalcite-like compound. In contrast, β-$Ni(OH)_2$ exhibits a well-ordered brucite type of the hydroxide layers [3]. $Ni(OH)_2$ has emerged as one of the most promising electrode materials for supercapacitor applications due to its low cost, well-defined electrochemical redox behavior, and high theoretical specific capacitance. Nevertheless, its electrochemical performance is limited by low electrical conductivity, low rate capability and poor cycling stability. From the previous work, $Ni(OH)_2$ combined with several types of carbonaceous materials has been reported. For example, Wang et al. [4] reported $Ni(OH)_2$ nanoflowers anchored on a 3D graphene-based hydrogel with a specific capacitance of 1632 F g^{-1} at 1 A g^{-1} and capacitance retention of ~95.2% at 4 A g^{-1} after 1000 cycles. Dong et al. [5] investigated the electrochemical performance of $Ni(OH)_2$ nanosheets supported on reduced graphene oxide and reported a specific capacitance of 1886 F g^{-1} at 5 A g^{-1}. Numan et al. [6] prepared $Ni(OH)_2$/graphite nanosheet composites produced via a homogeneoue precipitation method. The as-synthesized composite was reported with a specific capacitance of 1956 F g^{-1} at a current density of 1 A g^{-1}. To date, although several $Ni(OH)_2$/carbon-based composites have been reported with the enhanced electrochemical performance, few attempts have been made to use GQDs with the variation in domain sizes for the assembly of $Ni(OH)_2$ composites.

Herein, $Ni(OH)_2$/GQD composites were prepared by using a hydrothermal method and their electrochemical properties were systematically investigated. GQDs with the variation of particle sizes were synthesized by a pyrolysis approach. The electrochemical performance of all composites was investigated in comparison with $Ni(OH)_2$.

2. EXPERIMENTAL PROCEDURE

2.1 Materials

Citric acid was purchased from Merck. Polyvinylidene difluoride (PVDF) was used as received from Alfa

Aesar. Nickel acetate tetrahydrate, $Ni(CH_3COO)_2{\cdot}4H_2O$ and 1-methyl-2-pyrrolidinone (NMP) were purchased from Sigma-Aldrich. Urea and potassium hydroxide were obtained from Ajax Finechem. All reagents were used without any further purification.

2.2 Synthesis of GQDs with the variation of particle sizes

GQDs were prepared by controlling the carbonization with different reaction time (20 and 60 min) and the samples were denoted as G20 and G60, respectively. 2 g of citric acid was put into a round bottom flask and then heated to 200ºC using a heating mantle. After the melted product was cooled down, NaOH was added to stop the reaction and the yellow-to-dark brown colored solution was obtained. In order to precipitate the GQDs, a copious amount of ethanol was added and the GQD precipitates were separated by centrifugation. The as-obtained GQDs were then dried in vacuo at 60ºC.

2.3 Synthesis of $Ni(OH)_2$/GQD composites

0.2488 g of $Ni(CH_3COO)_2{\cdot}4H_2O$ and 0.24 g of urea were dissolved in aqueous solution and mixed with G20 with the variation of loading (10, 30, 60 and 90 mg of G20). The samples were denoted as NG20-1, NG20-3, NG20-6 and NG20-9, respectively. Then, the solution was continuously stirred to form a homogeneous solution. After that, the mixture was transferred into a Teflon-lined stainless steel autoclave and maintained at 150°C for 6 h. The autoclave was cooled to room temperature. The precipitates were collected and washed with distilled water and ethanol for several times. The final product was dried in a vacuum oven at 60°C. The $Ni(OH)_2$ was synthesized by following a similar procedure except no addition of GQDs in the mixture. For comparison, NG60-3 was also prepared by mixing with 0.2488 g of $Ni(CH_3COO)_2{\cdot}4H_2O$, 0.24 g of urea and 30 mg of G60 and the following procedure was similarly adopted as mentioned above.

2.4 Electrochemical measurements with a three-electrode cell

The electrochemical performance of all samples was evaluated by using a conventional three-electrode system. Three-electrode setup was composed of a working electrode (electroactive material), reference electrode (Ag/AgCl in 3 M KCl) and counter electrode (platinum plate 2.5×2.5 cm^2) in a 2.0 M KOH aqueous electrolyte. The active material was mixed with a polyvinylidene difluoride (PVDF) binder and carbon black in the mass ratio of 80:10:10 in N-methyl-2-pyrrolidone (NMP) to make a homogeneous slurry that was subsequently coated on the nickel foam substrate (1×1 cm^2). The as-prepared electrode was pressed at 10 MPa and then dried at 100°C for 12 h. The mass of the electroactive materials was approximately 1 mg. Cyclic voltammetry, galvanostatic charge/discharge and electrochemical impedance spectroscopy were measured by an autolab PGSTAT302N workstation. The amplitude was set at 5 mV with the operating frequency ranging from 0.01 Hz to 100 kHz. All the electrochemical measurements were operated at the cut-off voltage between 0 and 0.6 V versus Ag/AgCl for the cyclic voltammetry tests. The specific capacitance can be calculated from the galvanostatic discharge of a supercapacitor by using the following equation:

$$C_s\,(F\ g^{-1}) = \frac{2i_m \int V dt}{V^2 \Big|_{Vi}^{Vf}} \qquad (1)$$

where i_m = I/m (A g^{-1}) is the current density, I is the current, m is mass of the electroactive material, and V is the potential. V_i and V_f are initial and final potential values, respectively.

2.5 Material characterization

X-ray diffraction (XRD) patterns of $Ni(OH)_2$ and as-prepared $Ni(OH)_2$/GQD composites were obtained by using a Bruker D8 Advance wide angle X-ray diffractometer operated between 5° and 70° with Ni-filtered Cu K_α radiation of wavelength 1.5406 Å, 40 kV, and 40 mA. The QUANTA 450 instrument was used to examine the morphology of all samples. The samples were coated with Au prior to scanning electron microscope (SEM) operation. The size and zeta potential of the synthesized GQDs were analyzed by a Nano-ZS90 zetasizer.

3. RESULTS AND DISCUSSION

Fig. 1a shows the XRD pattern of $Ni(OH)_2$. The peaks located at 12.5°, 25.1°, 33.2°, 36.2° and 59.5° in the $Ni(OH)_2$ are crystallographically assigned to be (003), (006), (101), (015) and (110) planes, respectively. All of the reflection peaks are indexed to the hexagonal phase of α-$Ni(OH)_2$ (JCPDS 38-0715). The XRD pattern of $Ni(OH)_2$ exhibits the strong diffraction peaks of (003) and (006) at low angles, indicating the clear layered structure of the hydrotalcite phase. The high intensity of the (003) plane suggests that as-synthesized $Ni(OH)_2$ has high crystallinity. The main reactions involved in the synthetic system are as follows [7]

$$CO(NH_2)_2 + H_2O \leftrightarrow 2NH_3 + CO_2 \qquad (2)$$

$$Ni^{2+} + xNH_3 \leftrightarrow Ni(NH_3)_x^{2+} \qquad (3)$$

$$NH_3 + H_2O \leftrightarrow OH^- + NH_4^+ \qquad (4)$$

$$Ni^{2+} + 2OH^- \leftrightarrow Ni(OH)_2 \qquad (5)$$

Fig. 1b displays the XRD patterns of NG20 composites with various G20 loading contents and NG60-3. The XRD reflection peaks of NG20-1 are clearly sharp than those of other NG20 composites, which demonstrates more highly crystalline phase of NG20-1. It can be seen that the peak positions (003) of NG20-3, NG20-6 and NG20-9 show significant shifts toward the lower angle due to the various intercalated anions that exist in their interlayer spaces. On the contrary, the XRD pattern of NG60-3 exhibits the absence of (003) peak, indicating no long-range ordering along the c-axis of the layered $Ni(OH)_2$. In addition, the (002) reflection peak of graphite resulting from the GQD restacking is not observed at 2Θ of 26° in all NG composites, suggesting well-uniform dispersibility of GQDs with the $Ni(OH)_2$ matrix.

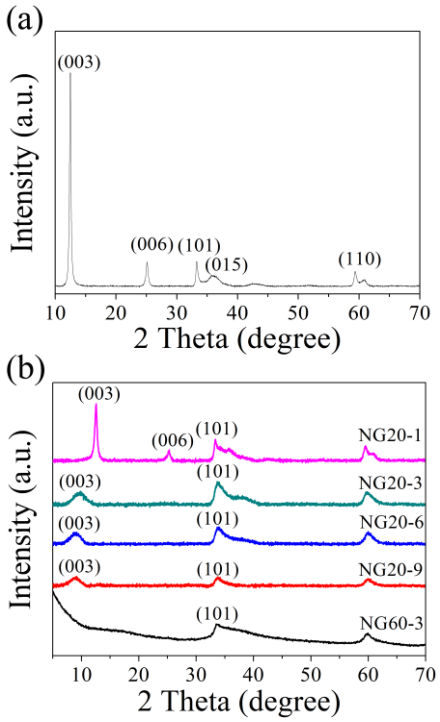

Fig. 1 XRD patterns of (a) $Ni(OH)_2$ and (b) NG20-1, NG20-3, NG20-6, NG20-9 and NG60-3.

The morphological studies of the $Ni(OH)_2$ and as-prepared NG composites were monitored by SEM as shown in Fig. 2. $Ni(OH)_2$ shows a rough surface with a flower-like structure and the thickness of nanopetals about 42 nm as seen in Fig. 2a. After combining with GQDs, the NG20-3 and NG60-3 still maintain the flower-like shape but the nanoflowers become more distorted than $Ni(OH)_2$, which is consistent with the broader (003) peak for NG20-3 and vanished (003) peak for NG60-3 in XRD. Furthermore, the distribution of the elements in the composite was analyzed by using the energy dispersive X-ray (EDX) spectroscopy mapping technique as shown in Fig. 2d. These results clearly indicate that the elements of Ni, O, and C are distributed homogeneously.

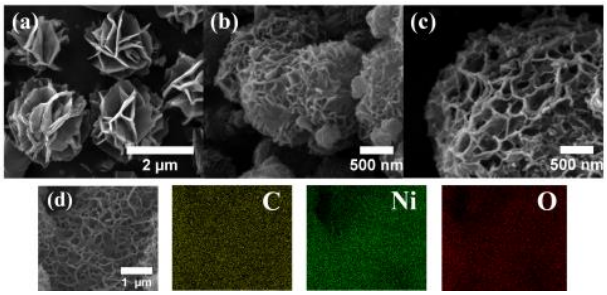

Fig. 2 SEM images of (a) $Ni(OH)_2$ (b) NG20-3 (c) NG60-3 and (d) EDX of NG60-3 for C, Ni and O.

Dynamic light scattering (DLS) was used to characterize the size of GQDs as summarized in Table 1. The average sizes of G20 and G60 are found to be 2.70 and 164.20 nm, respectively. Furthermore, the zeta potential of G20 and G60 shows the net negative charge due to many oxygen-functional groups. These negative charges of both G20 and G60 form the right ground for anchoring the positively charged $Ni(OH)_2$ nanoflowers by means of strong electrostatic interactions.

Table 1. The results from DLS analysis of GQDs

GQD	Average size (nm)	Zeta potential (mV)
G20	2.70	-3.36
G60	164.20	-52.93

Cyclic voltammograms (CV) and galvanostatic charge/discharge measurements were used to evaluate the electrochemical behavior of all samples. Fig. 3a shows the comparison between the CV curves of $Ni(OH)_2$ and NG composites at 5 mV s^{-1}. All CV curves reveal a pair of redox peaks, implying their predictable pseudocapacitive characteristics. For $Ni(OH)_2$, it is well-accepted that the surface redox reaction is derived from the following reaction: $Ni(OH)_2 + OH^- \leftrightarrow NiOOH + H_2O + e^-$. The presence of the anodic peak is attributed to the oxidation of $Ni(OH)_2$ to NiOOH, while the cathodic peak is related to the reverse reduction process. It can be seen that the areas under the CV curves of both NG20 and NG60 composites are larger than that of $Ni(OH)_2$, suggesting the enhanced specific capacitance of the composites. This result can be ascribed to a large surface area providing abundant efficient active sites for the transfer and diffusion as well as increase in wettability [8]. Besides, the potential difference between the anodic and cathodic peaks for NG composites is much smaller than that of $Ni(OH)_2$, confirming good reversibility of the faradaic reactions.

Fig. 3b illustrates the CV curves of NG20-3 electrodes collected at different scan rates from 1.0 to 50 mV s^{-1}. The result demonstrates that the oxidation peak and reduction peak of NG20-3 shift toward more positive and negative direction with increasing the scan rate which is attributed to the increase in the diffusion resistance within the active materials. Nevertheless, all CV curves do not get distorted in shape as the scan rate was raised, indicating good electrochemical stability of materials.

In Fig. 3c, the charge/discharge curves for the $Ni(OH)_2$ present a well-defined potential plateau at the given current density range, illustrating a typical pseudo-capacitive behavior. In Fig. 3d and 3e, the charge/discharge curves of the NG20-3 and NG60-3 show the similar shape compared to $Ni(OH)_2$. It can be seen that discharge time observed in NG20-3 and NG60-3 composites is longer than that of $Ni(OH)_2$, suggesting the a higher specific capacitance of 1487 F g^{-1} for NG20-3 and 1048 F g^{-1} for NG60-3 at 2 A g^{-1}. Meanwhile, NG60-3 with a larger GQD size provides lower specific capacitance compared to NG20-3. This might be due to the absence of long-range ordering of $Ni(OH)_2$. In addition, the specific capacitance decreases at high current density due to low accessibility of electrolyte ions to the surface of the electroactive materials.

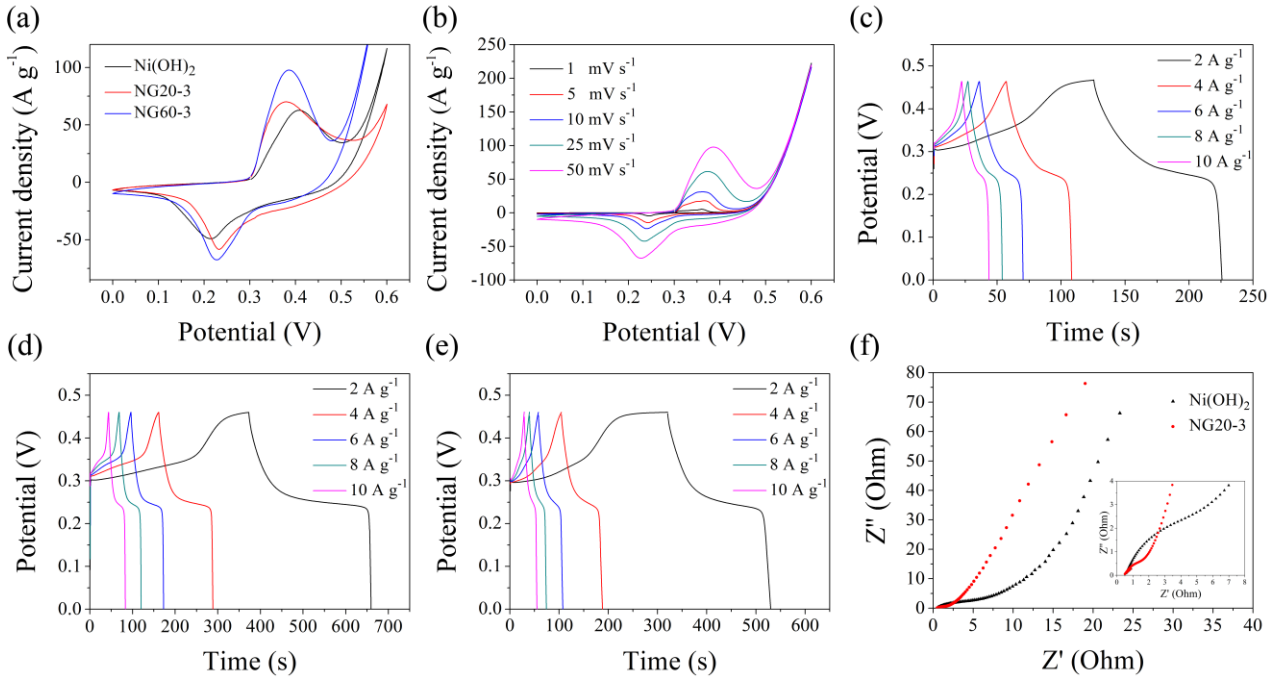

Fig. 3 CV curves of (a) $Ni(OH)_2$, NG20-3 and NG60-3 at scan rate 50 mV s^{-1} and (b) NG20-3 at different scan rates. The galvanostatic charge-discharge curves of (c) $Ni(OH)_2$, (d) NG20-3 and (e) NG60-3 at different current densities. (f) Nyquist plots of $Ni(OH)_2$ and NG20-3 and their magnified portion at high frequency (inset).

The Nyquist plots of the $Ni(OH)_2$ and NG20-3 are presented in Fig. 3f. The R_s, known as an equivalent series resistance, is defined as the sum of the resistance at electrolyte/electrode/current collector interfaces. The R_{ct} represents the resistance as a consequence of the charge transfer between active materials and electrolyte ions. The x-axis intercepts at the high frequency range represent the R_s and the diameter of the semicircle corresponds to the R_{ct} of the electrodes. It is found that the R_s of the NG20-3 and $Ni(OH)_2$ is 0.45 Ω and 0.48 Ω, respectively. Moreover, NG20-3 provides R_{ct} with 2.61 Ω which is considerably lower than R_{ct} of $Ni(OH)_2$ with 9.57 Ω, indicating the lower intrinsic resistance for NG20-3. The decreased R_{ct} observed in the composite is attributed to the presence of GQDs which can improve the electrical conductivity, confirming the superior electrochemical performance of the composite.

4. CONCLUSION

In conclusion, we successfully synthesized $Ni(OH)_2$/GQD composites via a hydrothermal method. The $Ni(OH)_2$/GQD composite with a small particle size of GQD exhibits the greater specific capacitance of 1487 F g^{-1} at a current density of 2 A g^{-1}.

5. ACKNOWLEDGEMENTS

This research was financially supported by Department of Chemistry, Faculty of Science, Kasetsart University and the Centre of Excellence in Chemistry for Innovation (PERCH-CIC). We also would like to acknowledge the Graduate School and Kasetsart University Research and Development Institute (KURDI) for financial support.

6. REFERENCES

[1] H. Wu, Y. Zhang, L. Cheng, et al., Graphene based architectures for electrochemical capacitors, Energy Storage Mater. 5 (2016) 8-32.

[2] Z. Zhang, J. Zhang, N. Chena, et al., Graphene quantum dots: an emerging material for energy-related applications and beyond, Energy Environ. Sci. 5 (2012) 8869-8890.

[3] J. Eskusson, A. Jänesa, A. Kikas, et al., Physical and electrochemical characteristics of supercapacitors based on carbide derived carbon electrodes in aqueous electrolytes, J. Power Sources. 196 (2011) 4109-4116.

[4] R. Wang, A. Jayakumar, C. Xu, et al., $Ni(OH)_2$ nanoflowers/graphene hydrogels: A new assembly for supercapacitors, ACS Sustainable Chem. Eng. 4 (2016) 3736-3742.

[5] X. Zang, C. Sun, Z. Dai, et al., Nickel hydroxide nanosheets supported on reduced graphene oxide for high-performance supercapacitors, J. Alloys Compd. 691 (2017) 144-150.

[6] J.T. Zhang, S. Liu, G.L. Pan, et al., A 3D hierarchical porous α-Ni(OH)2/graphite nanosheet composite as an electrode material for supercapacitors, J. Mater. Chem. A. 2 (2014) 1524-1529.

[7] G. Wei, K. Du, X. Zhao, et al., Carbon quantum dot-induced self-assembly of ultrathin $Ni(OH)_2$ nanosheets: A facile method for fabricating three-dimensional porous hierarchical composite micronanostructures with excellent supercapacitor performance, Nano. Res. 10 (2017) 3005-3017.

[8] S. Zhang, L. Sui, H. Dong, et al., High-performance supercapacitor of graphene quantum dots with uniform sizes, ACS Appl. Mater. Interfaces. 10 (2018) 12983-12991.